Antiviral activities of 4H-chromen-4-one scaffold-containing flavonoids against SARS–CoV–2 using computational and *in vitro* approaches

Vinit Raj, Jin-Hyung Lee, Jae-Jin Shim, Jintae Lee *

School of Chemical Engineering, Yeungnam University, 280 Daehak-Ro, Gyeongsan 38541, Republic of Korea

ABSTRACT

The widespread outbreak of the novel coronavirus called severe acute respiratory syndrome coronavirus-2 (SARS-CoV-2) has caused the main health challenge worldwide. This pandemic has attracted the attention of the research communities in various fields, prompting efforts to discover rapid drug molecules for the treatment of the life-threatening COVID-19 disease. This study is aimed at investigating 4H-chromen-4-one scaffold-containing flavonoids that combat the SARS-CoV-2 virus using computational and *in vitro* approaches. Virtual screening studies of the molecule's library for 4H-chromen-4-one scaffold were performed with the recently reported coronavirus main protease (M^{pro}, also called 3CL^{pro}) because it plays an essential role in the maturation and processing of the viral polyprotein. Based on the virtual screening, the top hit molecules such as isoginkgetin and afzelin molecules were selected for further estimating *in vitro* antiviral efficacies against SARS–CoV–2 in Vero cells. Additionally, these molecules were also docked with RNA-dependent RNA Polymerase (RdRp) to reveal the ligands-protein molecular interaction. In the *in vitro* study, isoginkgetin showed remarkable inhibition potency against the SARS-CoV-2 virus, with an IC$_{50}$ value of 22.81 μM, compared to remdesivir, chloroquine, and lopinavir with IC$_{50}$ values of 7.18, 11.63, and 11.49 μM, respectively. Furthermore, the complex stability of isoginkgetin with an active binding pocket of the SARS-CoV-2 M^{pro} and RdRp supports its inhibitory potency against the SARS-CoV-2. Thus, isoginkgetin is a potent leading drug candidate and needs to be used in *in vivo* trials for the treatment of SARS-CoV-2 infected patients.

© 2022 Elsevier B.V. All rights reserved.

1. Introduction

In the COVID-19 pandemic caused by the virulent nature of human coronavirus called severe acute respiratory syndrome coronavirus-2 (SARS-CoV-2) [1,2], the number of people infected globally is increasing rapidly [3-5]. In the current scenario, SARS-CoV-2 has caused>38 million COVID-19 cases and more than one million deaths globally (https://www.worldometers.info/coronavirus/) compared to the more virulent and less transmitted SARS-CoV outbreak in 2002–2003 (which caused only 800 cases and 774 deaths) [6]. Now, there is an urgent need for antiviral drug molecules to treat COVID-19 patients.

SARS-CoV-2 is a single-stranded RNA enveloped virus and encodes two overlapping viral polyproteins named pp1a and pp1ab. It has a 96.2% similarity with the SARS-CoV virus from the 2003 SARS epidemic in that both initiate angiotensin-converting enzyme 2 (ACE2) mediated entry into the host; both belong to the same *Nidovirales* virus family, and both originated

from the same part of China. Viral polyproteins are essential for viral replication and transcription. Viral encoded proteases include a papain-like protease (PL^{pro}), and the main protease (M^{pro}), also known as 3CL^{Pro}, where M^{pro} cleaves to the viral polyproteins at 11 positions, primarily at conserved Leu Gln↓ Ser Ala Gly↓ sequences, and leads to the assemblage of the viral replicase complex [7-9].

As a reported vital role of the SARS-CoV-2 M^{pro} in virus replication [10], the SARS-CoV-2 M^{pro} is an essential molecular drug target for the development and discovery of antiviral drug molecules against the novel coronavirus causing COVID-19. Equivalent cleavage specificity has not yet been described for human proteases, and thus, inhibition of the SARS-CoV-2 M^{pro} is unlikely to cause any toxicity in humans [11]. Recently, the X-ray structure of the SARS-CoV-2 M^{pro} has been elucidated (PDB ID: 6Y2F) [10], and this offers a means of discovering its inhibitors. In general, for the development or repurposing of the antiviral drug against the SAS-CoV-2, S protein, ACE2, TMPRSS2 (transmembrane protease serine 2) RNA-dependent RNA polymerase (RdRp), and PL^{pro} (papain-like protease) are also broadly considered as foremost targets for the antiviral drugs towards SARS likely SARS-CoV-2 and

* Corresponding author.
  E-mail address: jtlee@ynu.ac.kr (J. Lee).

other coronaviruses[12]. Some old drug molecules have been repurposed against the SARS-CoV-2 such as dexamethasone, remdesivir, and avifavir [13]. One of them, remdesivir is an adenosine analogue that inhibits viral RNA polymerase with RdRp. Hence, RdRp is another alternative target for the discovery and development of possible targeted molecules for the treatment of COVID-19 patients.

Moreover, in COVID-19 patients, it has been observed that inflammatory molecule levels (e.g. pro-inflammatory cytokines, IL-1β, IL-6, IL-7, IL-8, IL-9, IL-10, reactive protein fibroblast growth factor, granulocyte-colony-stimulating factor, IFN, tumor necrosis factor, granulocyte–macrophage colony-stimulating factor, macrophage inflammatory protein 1 α, and vascular endothelial growth factor) are higher in the cells of the lung, and lead to acute respiratory distress, severe injury, and death [14,15].

Because there are fewer options of marketed repurposed antiviral drugs against the SARS-CoV-2. Owing to the lack of toxicity of natural flavonoids, and the fact that their ability to synergize with conventional drug candidates was established, their functional groups easily interact with cellular targets, and they interrupt various pathways [16]. Thus, these features make flavonoids possible candidates for interacting with the coronavirus life cycle. From the chemical site, flavonoids have the hydroxylated phenolic group that is responsible for their antioxidant activity and are designed with two benzene rings (A- and B-rings) and linked with the heterocycle group pyrene scaffold (C-ring). As previously reported, various pharmacological activities of 4H–chromen-4-one synthetic scaffolds [17], and the significant advancement of natural flavonoids containing 4H-chromen-4-one scaffold have exhibited good antiviral, antibacterial, anti-inflammatory, anticancer, and antioxidant effects, and they also interrupt the RNA picornavirus and interfere with the replication cycle of DNA viruses [16,18,19]. Additionally, ginkgetin, isoginkgetin, and bilobetin are natural flavonoids that these molecules have the 4H-chromen-4-one scaffold and possess significant pharmacological activities [20-22]. Thus, the importance of all these pharmacological factors has attracted the attention of various research groups to discover and explore the role of 4H-chromen-4-one scaffolds against the current COVID-19 pandemic. Previous *in silico* studies of various flavonoids with the SARS-CoV-2 Mpro have recently been reported [23-28], which suggest that natural flavonoids might be effective drug molecules against SARS-CoV-2. In these previous studies, ginkgetin, isoginkgetin, and bilobetin are among a hundred hits, but no one has been yet reported any computational stabilities of isoginkgetin and afzelin with the SARS-CoV-2 Mpro or an antiviral *in vitro* assay against SARS-CoV-2.

4H–chromen-4-one containing flavonoids possess a broad range of biological activities including anti-inflammatory effectiveness [29]. Based on the previous anti-inflammatory role of H–chromen-4-one, we hypothesized that these molecules may be effective drug candidates for the treatment of COVID-19 because the level of the proinflammatory cytokines is high in the lung cells of COVID-19 patients [30]. Likewise, the recent advantage of the RdRp and SARS-CoV-2 Mpro targets in the translation of the viral RNA makes them important molecular targets for the development SARS-CoV-2 inhibitors. Additionally, the possible binding of 4H-chromen-4-one scaffold with RdRp and SARS-CoV-2 and its previous biological activities can make them an effective scaffold for the discovery of potential lead molecules against the COVID-19 pandemic. Consequently, 4H-chromen-4-one containing flavonoids maybe act not only suppressing the level of the proinflammatory cytokine in the lung cells of COVID-19 patients but also blocking the RdRp or SARS-CoV-2 Mpro active binding site, leading to inhibition of the translation of viral RNA. To corroborate this hypothesis, we performed virtual screening of a series of 4H–chromen-4-one containing flavonoids with the SARS-CoV-2 Mpro target. Further,

the higher binding energy molecules were selected and redocked with RdRp or SARS-CoV-2 Mpro to confirm the conformation binding. The molecular dynamic simulation was further performed to analyze the ligand-receptor complex conformation behavior in aqueous media. Additionally, density functional theory was used to reveal the reactivity of molecules. Finally, *in vitro* antiviral activities of two flavonoids (namely isoginkgetin and afzelin) were carried out against the SARS-CoV-2 in infected Vero cells. This is the first report on molecular simulation and *in vitro* antiviral activities of isoginkgetin, and afzelin.

2. Materials and methods

2.1. Ligands and SARS-CoV-2 Mpro protein collection

Ligands structures were collected from the PubChem library. The crystal structure of the SARS-CoV-2 Mpro protein (PDB: 6LU7) [31] and RNA-dependent RNA polymerase (RdRp), PDB: 6 M71 were retrieved from the RCSB protein database (https://www.rcsb.org/) at a resolution of 2.16, 2.90 Å, respectively [32]. To refine the proteins' structure, the proteins preparation wizards' tool of the Schrodinger suite was used. Extra co-crystallizing molecules of water were deleted, with the essential number of required hydrogens was included in the complex structure of the SARS-CoV-2, and RdRp proteins.

2.2. Preparation of ligands and structure-based virtual molecules screening

Two-dimensional structures of 4H-chromen-4-one containing flavonoids (total 96) were downloaded in a simulation description format (SDF) from the PubChem data bank (https://pubchem.ncbi.nlm.nih.gov/). Flavonoids structures were prepared using LigPrep tools of the Schrodinger suite, and all molecular structures were optimized over minimum energy to ensure the essential proper arrangement of molecules in space using a density functional theory (DFT) approach, Gaussian 09 suite [33,34]. Conformations and bond orders were minimized and refined using the OPLS 2005 force field [35]. After the energy minimization, all molecular structure was saved in pdb files. These prepared ligand libraries were subjected to analysis for structure-based virtual screening with an active binding pocket of the SARS-CoV-2 Mpro [36]. First, the active binding pocket of the SARS-CoV-2 Mpro was predicted by the CASTp server (Fig. 1). Also, the CASTp server predicted the active binding site of the SARS-CoV-2 Mpro was again confirmed by VINA random 25 runs between ligands and the SARS-CoV-2 Mpro (Fig. S1). Afterward, the predicted active site was assigned for the grid to the virtual screening, where drug molecules were treated as rigid entities although the assigned active pocket of the receptor was treated as a flexible entity [37,38]. To ensure the precision of docking results (such as reliability, validation, and reproducibility), a comparative study of molecular docking was achieved by two molecular docking methods, namely AUTO-DOCK [39] and VINA [40]. Also, binding energies, as well as ligand-receptor interactions, were revealed between natural flavonoids and the SARS-CoV-2 Mpro by the two computational approaches [39]. For the docking with RdRp protein, ARG553, THR556, THR687 and ALA685 was assigned active pocket. To capture the visualization of complex structure interactions of afzelin and isoginkgetin with the protein, BIOVIA Discovery Studio Visualizer was used.
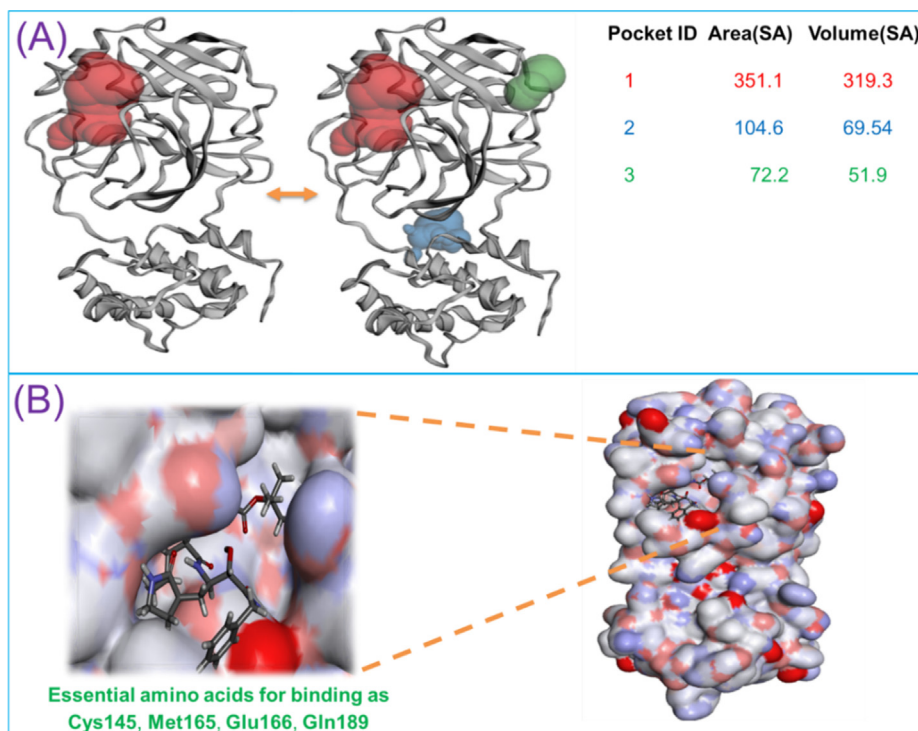
Fig. 1. Ribbon structures of the SARS-CoV-2 M^{pro}: (A) Possible ligand binding active site predicted by the CASTp server (http://sts.bioe.uic.edu/castp/index.html), where red indicates more suitable binding, whereas blue and green show a moderate conformation binding pocket. **(B)** The active binding cavity on the rigid surface of the SARS-CoV-2 M^{pro} with the interaction of α–ketoamide 13b (a positive control) as a previously reported potent inhibitor of SARS–CoV–2 [41].

2.3. ADME analysis

For the estimation of pharmacokinetic characteristics of top hit targeted molecules, we carried out ADME study using the QikProp software and swissADME, selecting as following properties; topological polar surface, gastrointestinal absorption, blood–brain barrier permeability, Lipinski violations, bioavailability score, Log Kp (skin permeation), and CYP1A2 inhibitor. An orally active pharmaceutical agent must not have molecular weight > 500 g/mol, LogP > 5, hydrogen-bond-donating atoms > 5, hydrogen-bond-accepting atoms > 10, and topological polar surface > 140.

2.4. Estimation of conformational stabilities of flavonoids with SARS-CoV-2 M^{pro} by molecular dynamic (MD) simulation

To analyze the conformation stabilities of isoginkgetin and afzelin with the SARS-CoV-2 M^{pro}, molecular dynamic simulations were carried out in an explicit water solution using YASARA dynamic software [42] on a SAMSUNG Intel Core i5-CPU with 4 GB RAM running the Windows 7 enterprise version (64-bit). The best molecular docking binding conformations of complexes were subjected to evaluation of their binding energy, as well as RMSD with the SARS-CoV-2 M^{pro}, over the MD run from 0 to 50.7 ns. For the complex structure of natural flavonoids with the SARS-CoV-2 M^{pro}, simulation cells were defined using periodic cell boundaries and were filled with an explicit water solvent at 0.997 g/L (density). A periodic simulation cell boundary, with a size of X = 61.30 A°, Y = 82.84 A°, and Z = 52.14 A°, was built around the whole complex system. The required amount of chloride and sodium ions was arbitrarily placed to attain the desire charge for the neutrality of the complex system. Pka values were only predicted for the sidechains of His, Asp, Lys, and Glu residues [43]. Initially, 298 K temperature was assigned and gradually increased to achieve equilibrium. Afterward, an AMBER14 molecular dynamic

force field was selected under physiological conditions at 0.9% NaCl, and pH 7.4 for MD simulation [44]. The total energy of the system was minimized initially via steepest descent minimization, as in a previously described method [45]. Finally, the complex system structure was submitted to an MD run of>100 ns at a 310 K, constant temperature, and 1 ps pressure. MD trajectories were saved for every 250 ps for further analysis. These MD trajectories were subjected to evaluate the RMSD of backbone, heavy atoms by the YASARA template file (md_analysis.mcr). Also, the binding energy of each conformation of complexes was analyzed by the YASARA template file (md_analyzebindenergy.mcr) [42]. The usual conformation stabilities of models were assessed from simulations and root means square deviations (RMSDs). According to the YASARA manual, free binding energies were analyzed without the participation of the entropy term. YASARA delivers positive binding energies, and thus, higher positive energies show favorable binding with a receptor in the assigned force field, although negative binding energies specify a weak binding. Finally, trajectory analysis data were found via MD simulation and denoted graphically using SigmaPlot 10.0. The flavonoids–SARS-CoV-2 M^{pro} binding conformation complexes were visualized using the Discovery Studio visualization software.

2.5. Structural stability of natural flavonoids determined by density functional theory

To optimize and evaluate the stability of the chemical structures of flavonoids, frontier molecular orbitals (FMOs) including lowest unoccupied molecular orbitals (LUMO), and highest occupied molecular orbitals (HOMOs) were analyzed using DFT [46]. Also, to determine the stability and reactivity of the orbitals of natural flavonoids, HOMO–LUMO energy gaps for flavonoid molecules were analyzed with the following equation [47]:

$$\Delta E = E_{LUMO} - E_{HOMO} \qquad (1)$$

Chemical hardness (η) and chemical potentials (μ) were calculated using the energy associated with HOMOs and LUMOs:

$$\mu = \frac{ELUMO + EHOMO}{2} \qquad (2)$$

$$\eta = \frac{ELUMO - EHOMO}{2} \qquad (3)$$

Electronegativity (χ) and electrophilicity (ω) were estimated by using ionization potentials (I), which are mostly defined as negative E_{HOMO} values, while electron affinity (A) was defined as being equal to negative E_{LUMO} values:

$$\chi = \frac{I + A}{2} \qquad (4)$$

$$\omega = \frac{\mu2}{2\eta} \qquad (5)$$

For optimization of flavonoid chemical structures, B3LYP level theory with acetone as a solvent media was used with a program of the Gaussian 09 suite, where a large gap between HOMO and LUMO orbitals showed better stability in the chemical structure of molecules, and the η value indicates the reactivity of a molecule, i.e. a higher value for η shows less reactivity of the chemical scaffold [46].

2.6. In vitro assessment of antiviral potency of natural flavonoids against SARS-CoV-2

The antiviral activities of flavonoids were estimated per a previously described method [48], and for this process, viral infected cells were used for antibodies specific to the viral nucleocapsid (N) protein. A dose–response curve (DRC) was made for individual compounds. The images were analyzed with immunofluorescence using Columbus software (Perkin Elmer). From the American Type Culture Collection (ATCC-CCL81), Vero cells were obtained for *in vitro* drug screening assays. Cells were maintained in Dulbecco's Modified Eagle's Medium (DMEM; Welgene) containing 1X antibiotic–antimycotic solution (Gibco) and 10% heat-inactivated fetal bovine serum (FBS) in a 5% CO_2 atmosphere at 37 °C. The SARS-CoV-2 virus (βCoV/KOR/KCDC03/2020) was obtained from the Korea Centers for Disease Control and Prevention (KCDC) and was propagated in Vero cells. Institute Pasteur South Korea supported this research, which was performed with the agreement of, and rules issued through, the Korea National Institute of Health (KNIH), South Korea, using Level 3 biosafety control procedures in laboratories approved for use by the KCDC.

2.7. Drug and reagents

Isoginkgetin (MW-566.51 g/mol), % purity $\geq$ 98% (HPLC) and afzelin (432.38 g/mol), % purity $\geq$ 90% (LC/MS-UV) were purchased from Sigma-Aldrich, and chloroquine, lopinavir, and remdesivir (used as reference compounds) were bought from Sigma-Aldrich, SelleckChem, and MedChemExpress, respectively. The anti-SARS-CoV-2 N protein antibody was purchased from Sino Biological Inc. (China), with Hoechst-33342 and the Alexa Fluor-488 goat anti-rabbit IgG (H + L) secondary antibody purchased from Molecular Probes. Also, paraformaldehyde (PFA) (a 32% aqueous solution) and normal goat serum were obtained from Vector Laboratories, Inc. (Burlingame, CA) and Electron Microscopy Sciences (Hatfield, PA), respectively. Chloroquine was mixed in Dulbecco's Phosphate-Buffered Saline (DPBS; Welgene). For *in vitro* studies, all reagents were well mixed in DMSO.

2.8. Dose-response curve analysis using an immunofluorescence method

DRC analysis was performed using the immunofluorescence method in the previously described protocol [48]. Briefly, 384-tissue culture μClear plates (Greiner Bio-One) were inoculated with Vero cells (1.2×10^4 cells/well) in a 1X antibiotic–antimycotic solution (Gibco) and DMEM containing 2% FBS in black, were permitted to stand for 24 h, and afterward, a 100 μM concentration of compounds was prepared at 10 points via serial dilution twice in DMSO. After 1 h, the compound treatment was moved into a BSL-3 containment facility, and plates were infected with SARS-CoV-2 added at a MOI of 0.0125 and kept at 37 °C for 24 h. Later, cells were fixed with a 4% PFA and an anti-SARS-CoV-2 nucleocapsid (N) primary antibody and treated with the Alexa Fluor 488-conjugated goat anti-rabbit IgG secondary antibody and Hoechst. Later, fluorescence images of infected cells were analyzed via immunofluorescence imaging using the Operetta system (Perkin Elmer). Images were acquired using Columbus software. The total number of cells in each well was calculated by the number of nuclei stained with Hoechst, and the number of infected cells was calculated as the number of cells expressing the N protein. Therefore, the infection ratio of the N protein was calculated as the number of expressed cells to the total number of cells. The infection ratios, cell numbers, and antiviral activity were normalized versus negative (0.5% DMSO) and positive (mock) controls. DRCs were fitted using the following sigmoidal dose–response model: Y = Bottom + (Top - Bottom)/(1 +(IC_{50}/X)^{Hillslope}), using Prism software. Finally, IC_{50} values were calculated from the normalized activity data set–fitted curves. IC_{50} and CC_{50} values were calculated in duplicate, and the quality of each assay was verified using the coefficients of variation and Z' factors.
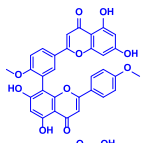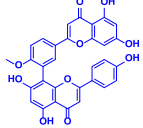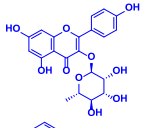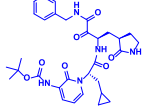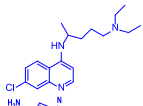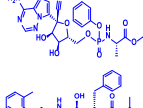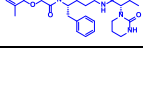
3. Results

3.1. Molecular docking of flavonoids with the SARS-CoV-2 M^{pro} to explore the molecular interactions

To reveal the interactions between natural flavonoids and the SARS-CoV-2 M^{pro}, we performed virtual screening of a series of 4H-chromen-4-one scaffold-containing natural flavonoids in total 96 (Table S1). The binding domain of the active pocket of the SARS-CoV-2 M^{pro} was confirmed by the CASTp server and random 25 dockings with the SARS-CoV-2 M^{pro}, where we found that domain 1 of SARS-CoV-2 is the main binding pocket for the drug molecules, which is similar to the previously reported positive control α-ketoamide 13b binding [41]. All 4H-chromen-4-one scaffold-containing molecules were screened with the same predicted active binding site of the SARS-CoV-2 M^{pro}, and as a result, all compound's binding affinities were found in the range −6.0 kcal/mol to −9.7 kcal/mol (VINA) (Table S1). Furthermore, redocking studies using AUTODOCK were carried out for three good binding flavonoids (below −9 kcal/mol) with the SARS-CoV-2 M^{pro}, showing that binding energies range between −11.3 and 13.5 kcal/mol (Table 1). Thus, three highly ranked flavonoids, such as isoginkgetin, bilobetin, and afzelin, were selected to reveal their interaction with the SARS-CoV-2 M^{pro}. For example, isoginkgetin exhibited good binding with the active binding domain of the SARS–CoV-2 M^{pro} at −13.58 kcal/mol, compared to positive control α-ketoamide (13b), chloroquine, remdesivir, and lopinavir at −9.50, −6.99, −9.13 and −8.93 kcal/mol, respectively. Also, it was found that isoginkgetin formed eight π-π bonds, and one hydrogen bond with amino acid residues Thr26, Gly113, Asn142, Cys145, His163, Met165, and Glu166 of the SARS-CoV-2 M^{pro}, which have common binding amino acid residues similar to those

Table 1

Molecular binding affinities of isoginkgetin, bilobetin, afzelin, α-ketoamide 13b, chloroquine, remdesivir, and lopinavir with the SARS-CoV-2 M^pro. Commonly observed amino acid residues are indicated in a blue font, where isoginkgetin, bilobetin, and afzelin are the test molecules while α-ketoamide 13b, [41] chloroquine, remdesivir, and lopinavir are a positive control.

| Name (PubChem ID)	Chemical structure	Binding energy: VINA (kcal/mol)	Binding energy: AUTODOCK (kcal/mol)	Interacting amino acids	Bonds
Isoginkgetin (5318569)		−9.38	−13.58	Thr26, Gly 113, Asn142, Cys145, His163, Met165, Glu166	8π-π, 1H
Bilobetin (5315459)		−9.75	−12.13	His41, Asn142, His163, Met165, Pro168, Gln189, Thr190, Gln192	6 π-π, 4H
Afzelin (5316673)		−9.02	−11.36	His41, Met165, Glu166, Asp187, Gln189	10π-π, 1H
α-Ketoamide 13b (PC)		−7.11	−9.50	His41, Cys145, Met165, Glu166, Leu167, Gln189	6 π-π, 6H
Chloroquine (PC)		−5.71	−6.99	Leu27, His41, Met49, Cys145, Met165, Glu166, Gln189	7 π-π,
Remdesivir (PC)		−7.89	−9.13	Asn142, Ser144, Cys145, His164, Glu166, Thr190	4 π-π, 6H
Lopinavir (PC)		−6.97	−8.93	Leu27, His41, Met49, Asn142, Gly143, Cys145, Pro168, Gyn189	9 π-π, 2H
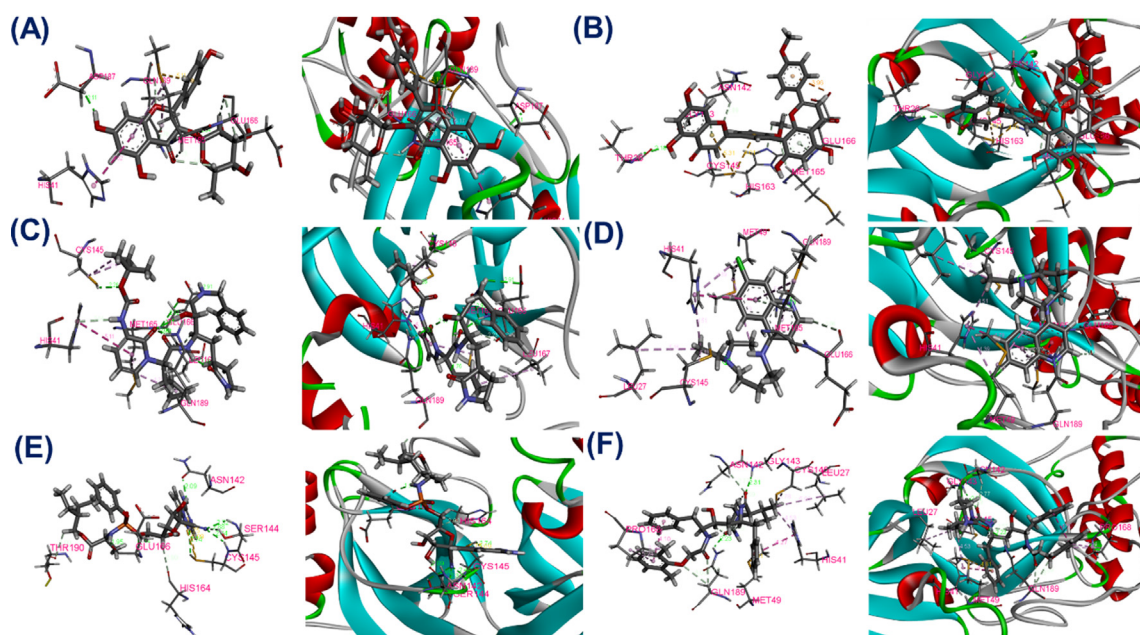
Fig. 2. Three-dimensional conformations of ligand-SARS-CoV-2 M^pro protein interactions for **(A)** Afzelin, **(B)** Isoginkgetin **(C)** α-Ketoamide 13b **(D)** Chloroquine, **(E)** Remdesivir, and **(F)** Lopinavir (positive control). Dotted green lines show hydrogen bonds between amino acid residues of the SARS-CoV-2 M^pro and ligands.

of positive controls Cys145, Met165, and Glu166 (Fig. 2). Additionally, isoginkogetin exhibited a better binding conformation compared with chloroquine, remdesivir, and lopinavir as shown in Table 1. Bilobetin and afzelin showed binding energies of −12.13 and −11.36 kcal/mol, respectively, along with bonds of six π-π, four hydrogens, and ten π-π, one hydrogen, compared to the positive control (at −9.50 kcal/mol). Isoginkgetin has a structural similarity with bilobetin, therefore among them, we have selected isoginkgetin and afzelin for further study. Importantly, molecular docking results collectively suggested that His42, Cys145, Met165, Glu166, and Gln189 are the common binding amino acids, which are required for binding with the active pocket domain of the SARS-CoV-2 M^pro (Table 1).

The inhibition constant (Ki_predicted) values of analyzed docking complexes were calculated by the following equation.

$$\Delta G = RT(Ki_{predicted})$$

$$Ki_{predicted} = e^{\Delta G/RT}$$

where gas constant R is 1.985×10^{-3} kcal mol^{-1} K^{-1}, ΔG is the binding energy of ligand-complex (kcal/mol), and room temperature T is 298.15 Kelvin.

The inhibitory constant Ki was found for isoginkgetin and afzelin are 22.94 and 19.19 μM, respectively.

Additionally, to discover the significant binding conformational of top three score molecules with the active pocket of RdRp, isoginkgetin, bilobetin, and afzelin were re-docked, and the result was compared with the three positive marketed drugs, chloroquine, remdesivir, and lopinavir. The binding affinities were estimated in terms of negative values. As shown in the Table S2, isoginkgetin exhibited the −8.30 kcal/mol binding energy with RdRp compared to the positive control. Remarkably, all three molecules along with three positive controls exhibited residence in the selective binding cavity of RdRp. On the other hand, redocking of targeted ligands also exhibited considerable alignment with the crystal structure of RdRp. Therefore, these findings suggested that docked ligand molecules occupied the selective pocket in the RdRp

as three molecules. Consequently, the used docking protocol endorses that identified ligands might work as a selective inhibitor of RdRp.

Likewise, each selected pose of 4H-chromen-4-one scaffold with RdRp was analyzed for binding affinity and molecular contraction between ligand and active pocket of the receptor, including hydrogen and π–π bonding with amino acid residues (Fig. 3.). Among all dock complexes, isoginkgetin-RdRp complex revealed the highest −8.30 kcal/mol docking score through the formation of hydrogen bonds and π–π interactions with RdRp amino acid residues (Table S2). While afzelin-RdRp showed −7.17 kcal/mol lowest docking score by a substantial contribution of 4 π–π and 4 hydrogen bonds interaction. Consequently, isoginkgetin has better conformational binding stability with the active domain of RdRp compared to afzelin. The molecular conformation binding of isoginkgetin with M^pro and RdRp suggests that isoginkgetin can bind with both targeted proteins.

3.2. Druggable pharmacokinetic profile

Regarding the estimation of molecules sorted from M^pro targeted library with their pharmacokinetic characteristic are shown in Table 2. Based on the calculated pharmacokinetic profile of targeted molecules isoginkgetin, bilobetin, and afzelin, a low level of gastrointestinal absorption was found. Additionally, the one violation of the Lipinski rule was shown by isoginkgetin, and bilobetin due to their > 500 g/mol molecular weight while afzelin exhibited the one violation of Lipinski rule owing to NH or OH > 5H-bond donors. As reported that 80 % of the compounds that fail to rule of five are not permeable while 48 % of those that pass are not permeable. All these tested compounds exhibited a considerable range of bioavailability scores. Hence, these parameters collectively indicate that these molecular are further needed to be investigated *in vivo* pharmacokinetic parameters.
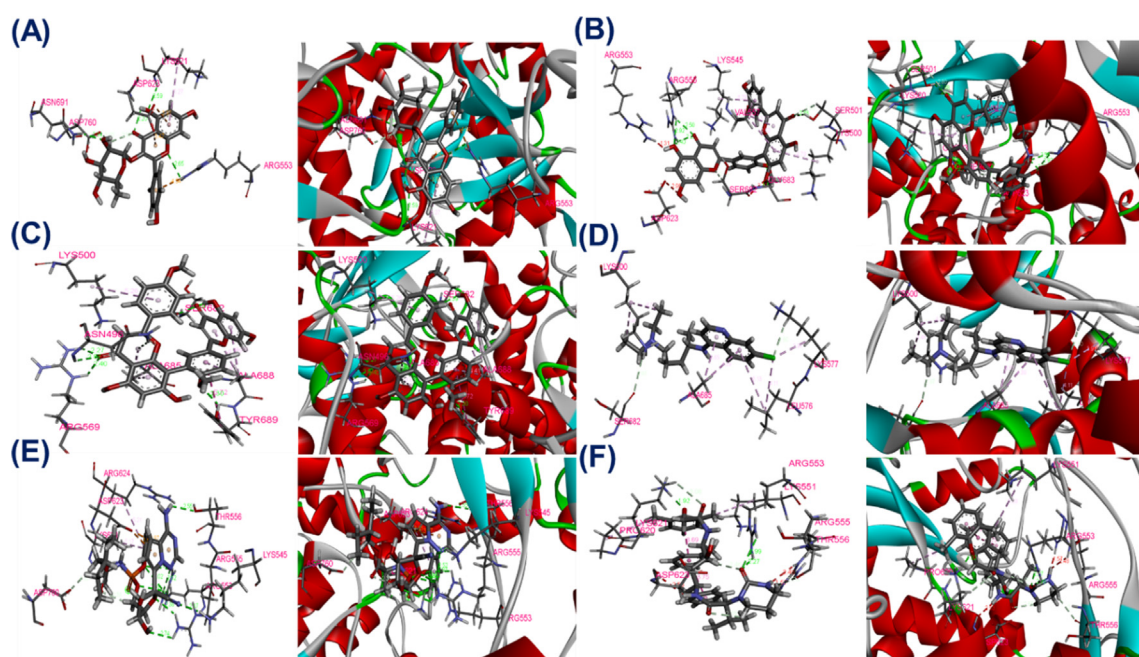

Fig. 3. Three-dimensional conformations of ligand-RdRp (PDB; 6 M71) protein interactions for **(A)** Afzelin, **(B)** Bilobetin, **(c)** Isoginkgetin, **(D)** Chloroquine, **(E)** Remdesivir, and **(F)** Lopinavir (positive control). Dotted green lines show hydrogen bonds between amino acid residues of the RdRp and ligands.

Table 2
Various physicochemical parameters of flavonoids to reveal the possible ADME properties.

Parameters	Value		
	Isoginkgetin	Bilobetin	Afzelin
Formula	$C_{32}H_{22}O_{10}$	$C_{31}H_{20}O_{10}$	$C_{21}H_{20}O_{10}$
Molecular weight	566.51 g/mol	552.48 g/mol	432.38 g/mol
H-bond acceptors	10	10	10
H-bond donors	4	5	6
Topological polar surface area	159.80 Å^2	170.80 Å^2	170.05 Å^2
Gastrointestinal absorption	Low	low	Low
Blood-brain barrier permeability	No	No	No
Lipinski violations	Yes; 1 violation: MW > 500	Yes; 1 violation: MW > 500	Yes; 1 violation: NH or OH > 5
Bioavailability score	0.55	0.55	0.55
Log K_p (skin permeation)	−5.72 cm/s	−5.86 cm/s	−8.07 cm/s
CYP1A2 inhibitor	No	No	No

3.3. Stability conformation study of natural flavonoids via density functional theory (DFT)

Density functional theory was used to determine the frontier molecular orbitals, the highest occupied molecular orbitals, and the lowest unoccupied molecule orbitals, of natural flavonoids. According to the FMO, the HOMO acts as an electron donor whereas the LUMO acts as an electron acceptor. To reveal the factor affecting such biological properties, molecular reactivities, ionization, and electron affinities of molecules, FMO theory for HOMOs and LUMOs is essential. Thus, it can be suggested that FMO studies can explore significant insights into the molecular mechanism of the active drug molecule. As a result of DFT calculations, isoginkgetin and afzelin showed a similar pattern of energy gaps between HOMOs and LUMOs of 4.15 and 4.18 eV, respectively (Table 3). The slightly similar energy gaps between both the isoginkgetin and afzelin the orbitals suggest that both molecules have similar stabilities. As shown in Fig. 4, the HOMO is located at the 5,7-dihydroxy-2-(4-hydroxyphenyl)-4H-chromen-4-one scaffold and the oxygen of the 2H-pyron ring, while the LUMO is at the 5,7-dihydroxy-2-(4-hydroxyphenyl)-4H-chromen-4-one scaffold of afzelin. For isoginkgetin, the HOMO is shown at 5,7-dihydroxy-2-(4-methoxyphenyl)-4H-chromen-4-one, and the LUMO is displayed at another similar 5,7-dihydroxy-2-(4-methoxyphenyl)-4H-chromen-4-one scaffold because isoginkgetin is the dimeric structure of two fused similar 5,7-dihydroxy-2-(4-methoxyphenyl)-4H-chromen-4-one scaffolds. Therefore, that suggests a single monomeric scaffold of isoginkgetin may participate in biological activity, while the other one, 7-dihydroxy-2-(4-methoxyphenyl)-4H-chromen-4-one scaffold may contribute to pharmacokinetic profiles due to the bulkiness of the isoginkgetin structure. Thus, 5,7-dihydroxy-2-(4-methoxyphenyl)-4H-chromen-4-one scaffold of isoginkgetin and afzelin will form an interaction with the active binding pocket of the SARS-CoV-2 M^{pro}, giving rise to the desired biological activity. As shown in Table 3, the reactivity order of molecules is as following; isoginkgetin > afzelin. The optimized structure of natural flavonoids shows that the oxygen of the pyron ring and the ketonic oxygen of the chromene ring have a higher electronic charge and a lower atomic charge at −0.47 and −0.49, respectively. Therefore, it is assumed that oxygen of the pyron ring and ketonic oxygen of the chromene ring are favored to interact with the positively charged atoms of amino acid residues of the active binding pocket of the receptor, compared to other oxygens atoms of isoginkgetin and afzelin rings.

Table 3
DFT calculation results of isoginkgetin and afzelin for quantum chemical parameters.

Quantum chemical parameters (eV)	Isoginkgetin	Afzelin
HOMO	−5.73	−5.66
LUMO	−1.58	−1.47
Energy gap (ΔE)	4.15	4.18
Chemical potential (μ)	−3.65	−3.56
Electron affinity (A)	1.58	1.47
Global hardness (η)	2.07	2.09
Ionization potential (I)	5.73	5.66
Electronegativity (χ)	3.65	3.56
Electrophilicity (ω)	3.20	3.03

3.4. Evaluation of flavonoid–SARS-CoV-2 M^{pro} complex stabilities via molecular dynamic (MD) simulation

In the solution medium, the motion and conformation stabilities of flavonoid–SARS-CoV-2 M^{pro} complexes were analyzed using MD simulation. The root-mean-square deviation (RMSD) and ligand binding energies were analyzed by using generated trajectories of ligand-receptor complexes overtime over>100 ns (Fig. 5). The average binding energies of isoginkgetin and afzelin were found to be 46.12 and 51.23 kcal/mol, respectively. These binding energies as per the selected force field suggested that isoginkgetin bound strongly with the SARS-CoV-2 M^{pro} throughout the MD runs compared to afzelin. Isoginkgetin–SARS-CoV-2 M^{pro} complexe showed equilibrium in trajectories after 60 ns and indicated RSMD complex stability during the 100 ns MD run. While afzelin–SARS-CoV-2 M^{pro} complex exhibited more backbone fluctuation during MD run. The binding energies of the afzelin complex showed relatively high fluctuations (-100 to 300 kcal/mol) compared to isoginkgetin (-100 to 200 kcal/mol), indicating the afzelin complex with the SARS-CoV-2 M^{pro} has less stable conformational over 100 ns during MD run. The RMSD backbone of isoginkgetin–SARS-CoV-2 M^{pro} has better conformation stability compared to the afzelin–SARS-CoV-2 M^{pro} complex. Supporting the isoginkgetin was tightly bound with the active pocket SARS-CoV-2 M^{pro}. Additionally, the stability profiles of the SARS-CoV-2 M^{pro} with isoginkgetin and afzelin complexes from the MD simulation are represented in Fig. 5, where the starting complex poses of isoginkgetin was similar to the last complex binding pose, while afzelin was dissimilar to the binding position in the initial and last complex poses (Fig. 5E, F). These observations suggest that isoginkgetin is the stable molecule with the active binding domain of the SARS-CoV-2 M^{pro}.

3.5. Assessment of in vitro antiviral potencies of isoginkgetin and afzelin against the SARS–CoV-2 virus

According to the virtual screening results of flavonoids with the SARS-CoV-2 M^{pro}, two natural flavonoids, isoginkgetin and afzelin, were assigned to be evaluated for their in vitro antiviral activities using SARS-CoV-2–infected Vero cells, as previously reported [48]. Confocal microscope images of the viral N protein and the cell nuclei were evaluated using the Operetta system (Parkin Elmer), and a DRC was estimated for each distinct tested molecule (Fig. 6). Three standard drugs (chloroquine, remdesivir, and lopinavir) were used as positive controls; they have an IC$_{50}$ of 11.63, 7.18, and 11.49 μM, respectively, which is similar to earlier reported studies [48]. Isoginkgetin exhibited remarkable antiviral activity against SARS-CoV-2 (an IC$_{50}$ value of 22.81 μM) compared to the three positive controls (IC$_{50}$ values from 7.18 to 11.63 μM). However, afzelin showed an IC$_{50}$ of>100 μM against SARS-CoV-2 (i.e., it showed ineffectiveness against SARS-CoV-2). Isoginkgetin also exhibited higher inhibition of the SARS-CoV-2 virus at a concentra-
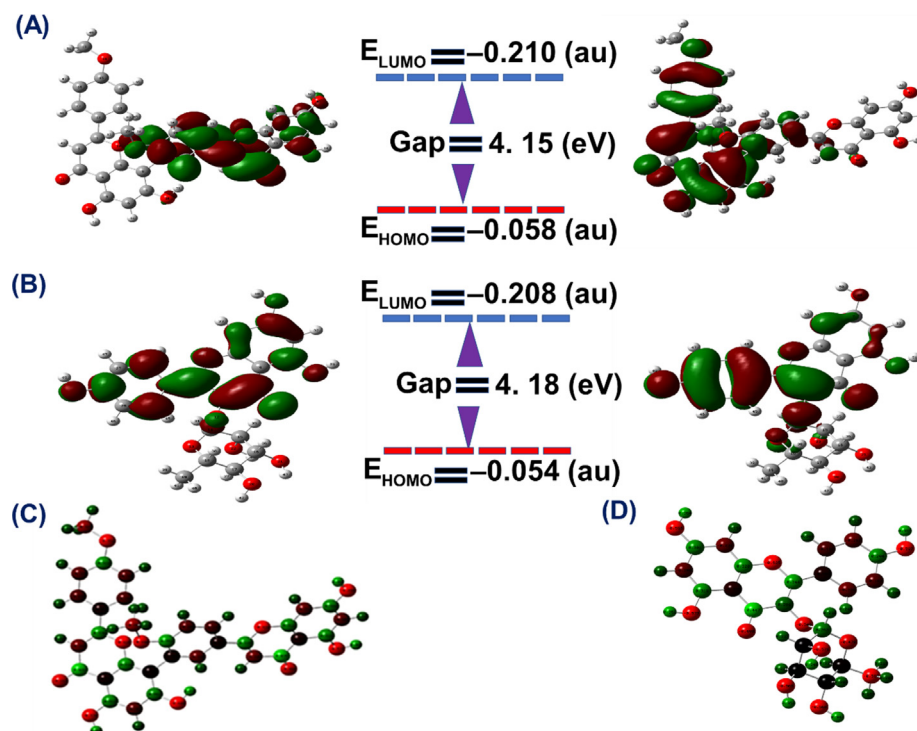
Fig. 4. Optimized molecular geometries differentiated into LUMO and HOMO, along with the energy gap of **(A)** isoginkgetin and **(B)** afzelin, were calculated using the DFT approach, and the optimized structures of **(C)** isoginkgetin and **(D)** afzelin are labeled with the atomic numbering of the electron distribution around the respective molecules.
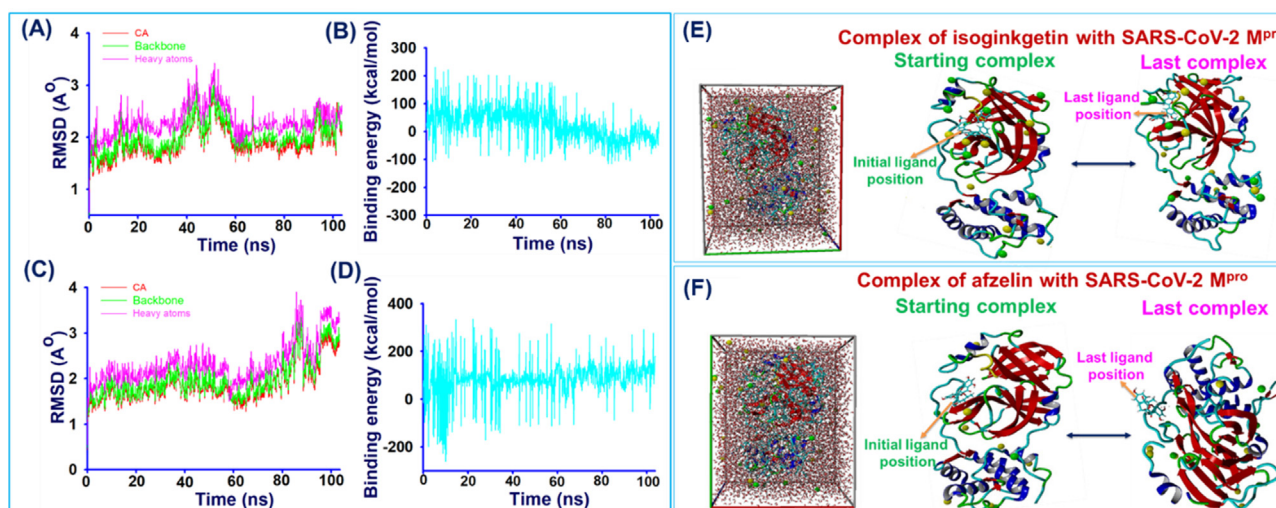

Fig. 5. The plots show the stability study of the interactions between afzelin, isoginkgetin, and SARS-CoV-2 M^{pro} complexes in an MD simulation over time, respectively. **(A-B)** RMSD and binding energy profiles of isoginkgetin–SARS-CoV-2 M^{pro} complex estimation during the MD simulation, determined using YASARA. **(C-D)** RMSD and binding energy profiles of afzelin–SARS-CoV-2 M^{pro} complex estimation during the MD simulation using YASARA. CA is C^α atoms of proteins while heavy atoms are all except hydrogen. The comparative binding positions of flavonoid–SARS-CoV-2 M^{pro} complexes were analyzed before and after long runs of MD simulations for **(E)** isoginkgetin and **(F)** afzelin with the SARS-CoV-2 M^{pro}.

tion of 50 μM (∼84 %), and the Vero cell survival ratio was ∼ 61% (Fig. 6). Also, it was noticed that inhibition of the SARS-CoV-2 virus increased with increased concentrations (at a 100 μM concentration, ∼90% inhibition), but the host cell survival ratio slightly decreased at a concentration of 100 μM (∼50%). Therefore, ∼50 μM of isoginkgetin is relatively safe for inhibiting the SARS-CoV-2 *in vitro*.

4. Discussion

With the rapid global spread of the COVID-19 pandemic, there are still limited options for the treatment of infected patients [49], leading to attention from the scientific community and efforts to discover a rapid alternative drug molecule for the treatment of COVID-19. In the present work, we attempted to discover potent flavonoid drug molecules against SARS-CoV-2, because natural flavonoid molecules have a broad range of biological activities with minimal, or no cytotoxicity [50]. We repurposed natural flavonoids for antiviral potency against SARS-CoV-2 using computational and *in vitro* approaches. From the computational studies, we found that isoginkgetin, bilobetin, and afzelin showed better binding with the well-known SARS-CoV-2 M^{pro} active binding pocket, and these results were compared to the previously reported M^{pro} inhibitor namely α-ketoamide 13b
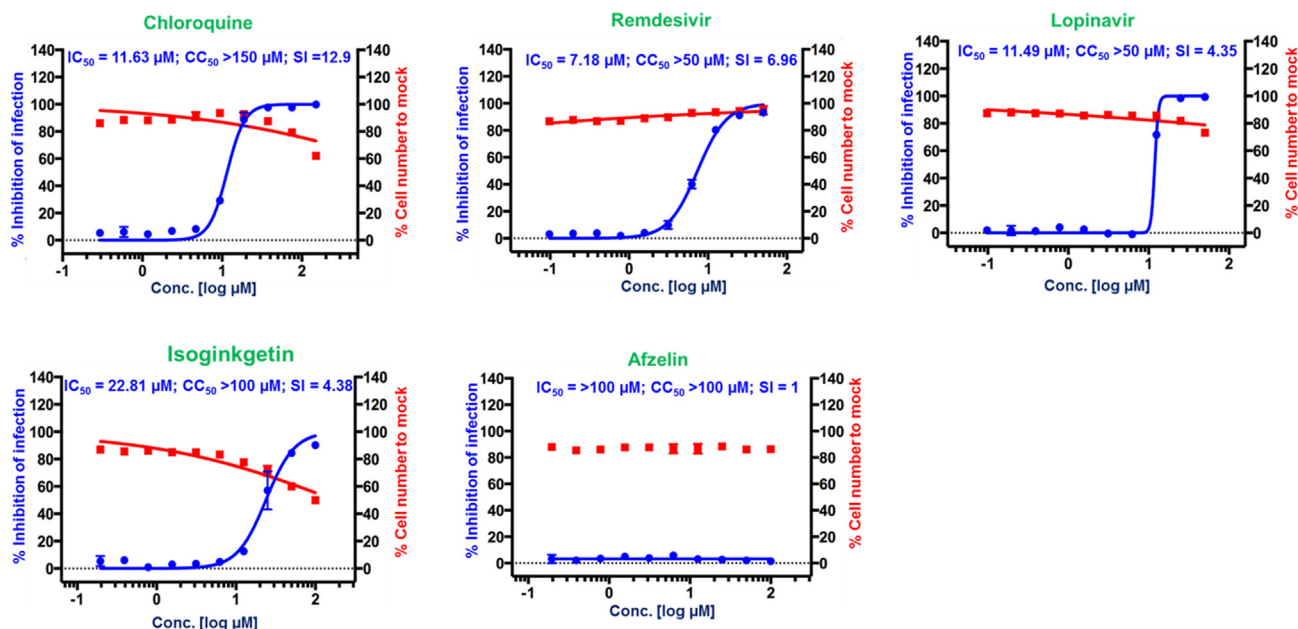
Fig. 6. Dose-response curve analysis of three control drugs (chloroquine, remdesivir, and lopinavir) and the two flavonoids (isoginkgetin and afzelin). The blue line represents inhibition of SARS-CoV-2 infection (%) and the red line denotes Vero cell viability (%). Mean ± SD was calculated from the results in duplicate experiments. All values are in μM, where IC_{50}, CC_{50}, and SI mean 50% inhibition, 50% cytotoxicity, and selectivity index, respectively.
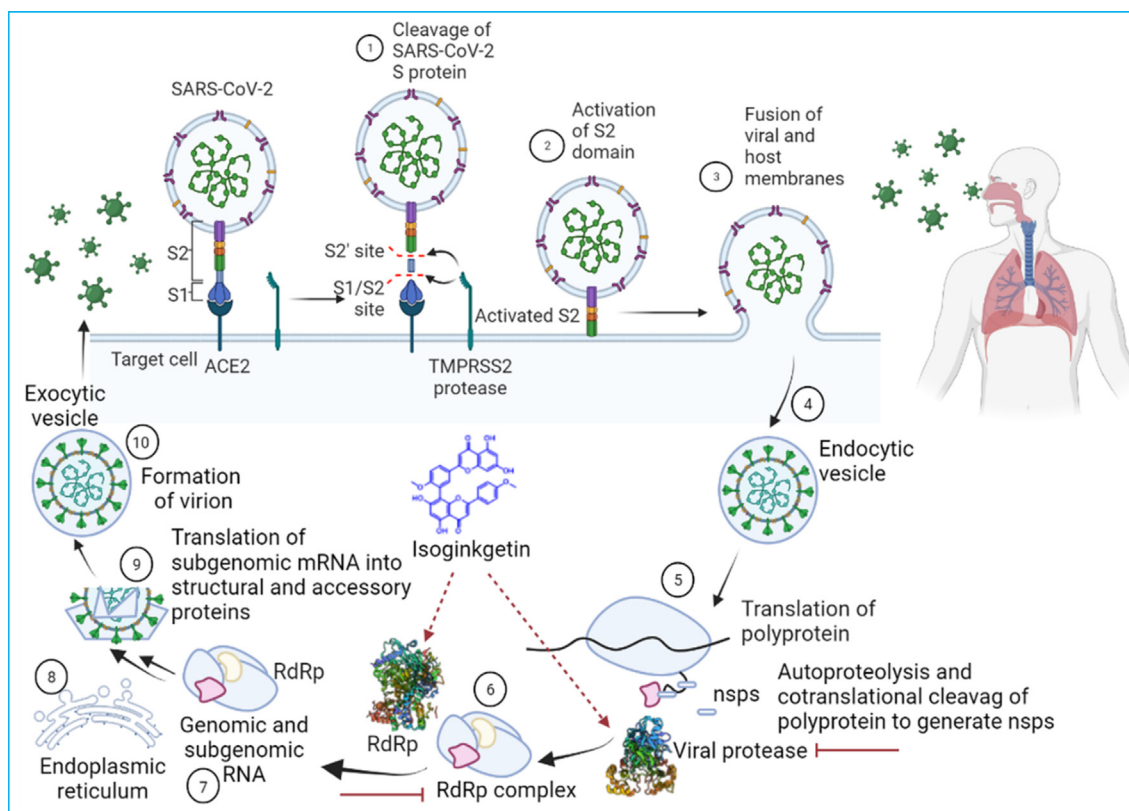

Fig. 7. A plausible mechanism of isoginkgetin binds with SARS-CoV-2 M^{pro} and RdRp; Structure features of SARS-CoV-2 and its main SARS-CoV-2 M^{pro}, where the main SARS-CoV-2 M^{pro} plays an important role in host lung cells for releasing SARS-CoV-2 RNA and translation of the viral genome RNA to produce viral replicase polyproteins pp1a and 1ab and their subsequent cleavage by viral proteinases into small viral proteins. Furthermore, viral proteins and genome RNA gather into virions in the ER and Golgi. Additionally, RdRp forms RdRp complex and with genomic and subgenomic RNA and leads to the translation of subgenomic mRNA into structural and necessary proteins. Consequently, forming the virion such as SARS-CoV-2 and transported in vesicles to the extracellular compartment [32].

[41]. On the other hand, isoginkgetin shows substantial complex stability after 60 ns in MD simulation with the active binding pocket of the SARS-CoV-2 M^{pro} (Fig. 5) and also exhibits chemi-

cal structural stability during the DFT calculation. Based on *in silico* results and structure similarity between bilobetin, and isoginkgetin, two molecules such as isoginkgetin and afzelin

have been selected for further *in vitro* antiviral assays (Table 1 and Fig. 6). Among two flavonoids, *in vitro* antiviral assay, iso-ginkgetin showed remarkable antiviral activity against SARS-CoV-2, and the result was compared with three marketed drugs as positive controls such as chloroquine, remdesivir, and lopinavir (Fig. 6). A recent study reported that isoginkgetin affects pre-mRNA splicing may be modulating RNA polymerase elongation rates [51,52]. Based on this previous report[53] of isoginkgetin effect towards pre-mRNA splicing and our current study about the effectiveness of isoginkgetin towards the SARS-CoV-2 suggest that isoginkgetin can be an effective drug candidate for the development of COVID-19 inhibitor. Additionally, the earlier reported anti-inflammatory activity of isoginkgetin, by activating a macrophage suggests that might be a better alternative to reduce the inflammatory markers in the lung[54]. Because inflammatory cytokines are high in the lung cell of COVID-19 patients. To confirm the further anti-inflammatory activity of isoginkgetin towards the lung cells, *in vitro* and *in vivo* anti-inflammatory studies are needed. Although, 12–18 mg/kg doses of isoginkgetin were reported safer *in vivo* in an animal model for the treatment of cancer [55]. Hence, collectively previous reports and our current study outcomes suggested that isoginkgetin might work against the SARS-CoV-2 [54,55]. Thus, further *in vivo* estimation of isoginkgetin against the COVID-19 is part of future interest.

Based on previous biological activities and current COVID-19 research, the plausible mechanism of isoginkgetin can be suggested to inhibit the SARS-CoV-2 because it is well known that the structural features of SARS-CoV-2 contain several proteins like spike glycoprotein (S), the SARS-CoV-2 M^pro, chymotrypsin-like main protease, RNA polymerase, and papain-like protease (Fig. 7) [56]. The S-protein of SARS-CoV-2 initiates host viral entry through binding with an ACE2 (cellular receptor) using an endosomal pathway [57-59], which leads to the release of viral RNA. Importantly, remdesivir was reproposed for targeting RNA-dependent RNA polymerase (RdRp) and inhibits the viral RNA synthesis [60]. The critical role of this enzyme in the viral lifecycle, RdRp is an attractive target for the treatment of COVID-19. The molecular docking result of the current study reveals the binding interaction of the targeted molecule with RdRp. For the support of this interaction study, *in vivo* study is part of interest.

The released viral RNA starts the viral translation by converting the viral genome RNA into replicase polyproteins 1ab and pp1a, which are cleaved by the SARS-CoV-2 M^pro and a papain-like protease into essential small viral proteins (Fig. 7). Furthermore, genome RNA and viral proteins accumulate into virions in the ER and Golgi, and SARS-CoV-2 is transported in vesicles to the extracellular compartment. Throughout this process, M1 pro-inflammatory macrophages and T-helper cells secrete interleukins and induce inflammation inside lung cells [61,62]. Thus, the significant role of SARS-CoV-2 M^pro protein in the translation process of viral RNA inside side the host cell is another prominent drug target. Although there is no similar viral protease in the host identified yet. Consequently, SARS-CoV-2 M^pro targeted inhibitors highly exert selectivity towards SARS-CoV-2 instead of human cells. The result of molecular docking of our present study suggests that isoginkgetin shows a better binding affinity with SARS-CoV-2 M^pro.

With the above-mentioned important role of the SARS-CoV-2 M^pro and RdRp in viral translation, and the current collective consequences of our computational molecular docking, ADME, DFT, MD simulation, and the *in vitro* antiviral potencies of isoginkgetin against SARS–CoV-2, it can be predicted that M^pro and RdRp are a target for isoginkgetin. It would be fascinating to verify this prediction *in vivo*.

5. Conclusion

In summary, this study was conducted to repurpose natural flavonoids for antiviral activity against SARS-CoV-2. Combining several computational tools and *in vitro* effectiveness of isoginkgetin against SARS-CoV-2 in infected Vero cells, we can conclude that isoginkgetin has antiviral activity against SARS-CoV-2 and further molecular binding interaction revealed that isoginkgetin can bind with the active pocket domain of SARS-CoV-2 M^pro or RdRp against SARS-CoV-2 and may inhibit the active binding pocket of these targeted proteins. These outcomes collectively support our purposed hypothesis that 4H-chromen-4-one scaffold containing isoginkgetin might work as an effective drug candidate against the SARS-CoV-2, *in vitro* and further conformation binding of isoginkgetin revealed the binding pattern with M^pro or RdRp proteins. These facts are useful to understand the mechanistic aspects to inhibit viral protein translation, participating in SARS-CoV-2 M^pro or RdRp by screened ligands and support to understand the stability and interaction of protein-ligands complexes. The current *in vitro* efficacy of isoginkgetin as an antiviral agent and conformation interaction studies collectively suggest that isoginkgetin may be used as a potential molecule to develop the antiviral drug against the SARS-CoV-2.

Declaration of Competing Interest

The authors declare that they have no known competing financial interests or personal relationships that could have appeared to influence the work reported in this paper.

Appendix A. Supplementary material

Supplementary data to this article can be found online at https://doi.org/10.1016/j.molliq.2022.118775.

References

[1] W. Vuong, M.B. Khan, C. Fischer, E. Arutyunova, T. Lamer, J. Shields, H.A. Saffran, R.T. McKay, M.J. van Belkum, M.A. Joyce, H.S. Young, D.L. Tyrrell, J.C. Vederas, M.J. Lemieux, Feline coronavirus drug inhibits the main protease of SARS-CoV-2 and blocks virus replication, Nat. Commun. 11 (1) (2020), https://doi.org/10.1038/s41467-020-18096-2.
[2] S. Khan, B. Shaker, S. Ahmad, S.W. Abbasi, M. Arshad, A. Haleem, S. Ismail, A. Zaib, W. Sajjad, Towards a novel peptide vaccine for Middle East respiratory syndrome coronavirus and its possible use against pandemic COVID-19, J. Mol. Liq. 324 (2021) 114706, https://doi.org/10.1016/j.molliq.2020.114706.
[3] Q. Li, Z. Wang, Q. Zheng, S. Liu, Potential clinical drugs as covalent inhibitors of the priming proteases of the spike protein of SARS-CoV-2, Comput. Struct. Biotechnol. J. 18 (2020) 2200.
[4] L.T. Phan, T.V. Nguyen, Q.C. Luong, T.V. Nguyen, H.T. Nguyen, H.Q. Le, T.T. Nguyen, T.M. Cao, Q.D. Pham, Importation and human-to-human transmission of a novel coronavirus in Vietnam, N. Engl. J. Med. 382 (2020) 872.
[5] S. Ahmad, Y. Waheed, S. Ismail, S.W. Abbasi, M.H. Najmi, A computational study to disclose potential drugs and vaccine ensemble for COVID-19 conundrum, J. Mol. Liq. 324 (2021) 114734, https://doi.org/10.1016/j.molliq.2020.114734.
[6] L. Fu, F. Ye, Y. Feng, F. Yu, Q. Wang, Y. Wu, C. Zhao, H. Sun, B. Huang, P. Niu, Both Boceprevir and GC376 efficaciously inhibit SARS-CoV-2 by targeting its main protease, Nat. Commun. 11 (2020) 1.
[7] T. Pillaiyar, M. Manickam, V. Namasivayam, Y. Hayashi, S.-H. Jung, An overview of severe acute respiratory syndrome–coronavirus (SARS-CoV) 3CL protease inhibitors: peptidomimetics and small molecule chemotherapy, J. Med. Chem. 59 (2016) 6595.
[8] A. Khan, M.T. Khan, S. Saleem, M. Junaid, A. Ali, S.S. Ali, M. Khan, D.-Q. Wei, Structural Insights into the mechanism of RNA recognition by the N-terminal

RNA-binding domain of the SARS-CoV-2 nucleocapsid phosphoprotein, Comput. Struct. Biotechnol. J. 18 (2020) 2174–2184.

[9] A. El-Hoshoudy, Investigating the potential antiviral activity drugs against SARS-CoV-2 by molecular docking simulation, J. Mol. Liq. 318 (2020) 113968.

[10] W. Dai, B. Zhang, X.-M. Jiang, H. Su, J. Li, Y. Zhao, X. Xie, Z. Jin, J. Peng, F. Liu, Structure-based design of antiviral drug candidates targeting the SARS-CoV-2 main protease, Science 368 (2020) 1331.

[11] H. Sies, M.J. Parnham, Potential therapeutic use of ebselen for COVID-19 and other respiratory viral infections, Free Radic. Biol. Med. 156 (2020) 107–112.

[12] A. Zumla, J.F.W. Chan, E.I. Azhar, D.S.C. Hui, K.-Y. Yuen, Coronaviruses-drug discovery and therapeutic options, Nat. Review. 15 (5) (2016) 327–347.

[13] T.R.C Group, Dexamethasone in Hospitalized Patients with Covid-19 — Preliminary Report, N. Engl. J. Med. (2020), https://doi.org/10.1056/NEJMoa2021436.

[14] S. Gangemi, A. Tonacci, AntagomiRs: A novel therapeutic strategy for challenging COVID-19 cytokine storm, Cytokine Growth F. R. 58 (2020) 111–113.

[15] B. Burgos-Blasco, N. Güemes-Villahoz, J.L. Santiago, J.I. Fernandez-Vigo, L. Espino-Paisán, B. Sarriá, J. García-Feijoo, J.M. Martinez-de-la-Casa, Hypercytokinemia in COVID-19: Tear cytokine profile in hospitalized COVID-19 patients, Exp. Eye Res. 200 (2020) 108253, https://doi.org/10.1016/j.exer.2020.108253.

[16] M. Russo, S. Moccia, C. Spagnuolo, I. Tedesco, G.L. Russo, Roles of flavonoids against coronavirus infection, Chem. Biol. Interact. 328 (2020) 109211, https://doi.org/10.1016/j.cbi.2020.109211.

[17] V. Raj, J. Lee, 2H/4H-Chromenes—A versatile biologically attractive scaffold, Frontiers in Chemistry 8 (2020).

[18] S. Lalani, C.L. Poh, Flavonoids as antiviral agents for Enterovirus A71 (EV-A71), Viruses 12 (2020) 184.

[19] S.B. Ghag, V.S. Adki, T.R. Ganapathi, V.A.J.B. Bapat, B. Engineering, Plant Platforms for Efficient Heterologous Protein Production, Biotech. Bioprocess Eng. 26 (2021) 546–567.

[20] V.S. Gontijo, M.H. Dos Santos, C. Viegas Jr, Biological and chemical aspects of natural biflavonoids from plants: a brief review, Mini. Rev. Med. Chem. 17 (2017) 834–862.

[21] K. Miki, T. Nagai, K. Suzuki, R. Tsujimura, K. Koyama, K. Kinoshita, K. Furuhata, H. Yamada, K.J.B. Takahashi, M.C. letters, Anti-influenza virus activity of biflavonoids. Bioorg Med. Chem. Lett. 17 (2007) 772-5

[22] I. Ishola, J. Chaturvedi, S. Rai, N. Rajasekar, O. Adeyemi, R. Shukla, T.J.J.o.e. Narender, Evaluation of amentoflavone isolated from Cnestis ferruginea Vahl ex DC (Connaraceae) on production of inflammatory mediators in LPS stimulated rat astrocytoma cell line (C6) and THP-1 cells, J. Ethnopharmacol. 146 (2013) 440–448.

[23] N. Chitranshi, V.K. Gupta, R. Rajput, A. Godinez, K. Pushpitha, T. Sheng, M. Mirzaei, Y. You, D. Basavarajappa, V. Gupta, Evolving geographic diversity in SARS-CoV2 and in silico analysis of replicating enzyme 3CLPro targeting repurposed drug candidates, J. Transl. Med. 278 (2020), https://doi.org/10.1186/s12967-020-02448-z.

[24] S. Rana, S. Sharma, K.S. Ghosh, Virtual screening of naturally occurring antiviral molecules for SARS-CoV-2 mitigation using docking tool on multiple molecular targets, Cambridge Open Engage, ChemRxiv. Cambridge, 2020.

[25] B.G. Vijayakumar, D. Ramesh, A. Joji, T. Kannan, In silico pharmacokinetic and molecular docking studies of natural flavonoids and synthetic indole chalcones against essential proteins of SARS-CoV-2, Eur. J. Pharmacol. 886 (2020) 173448.

[26] I.E. Orhan, F.S. Senol Deniz, Natural Products as Potential Leads Against Coronaviruses: Could They be Encouraging Structural Models Against SARS-CoV-2? Nat, Products Bioprospect. 10 (4) (2020) 171–186.

[27] H. Gowtham, D. Monu, Y. Ajay, C. Gourav, R. Vasantharaja, K. Bhani, S. Koushalya, S. Shazia, G. Priyanka, C. Leena, Exploring structurally diverse plant secondary metabolites as a versatile source of drug targeting different molecular mechanisms of Severe Acute Respiratory Syndrome Coronavirus-2 (SARS-CoV-2) pathogenesis: An in silico approach. Research Square. (2020). 10.21203/rs.3.rs-27313/v1

[28] B. Benarba, A. Pandiella, Medicinal plants as sources of active molecules against COVID-19, Front. Pharmacol. 11 (2020).

[29] M. Hämäläinen, R. Nieminen, P. Vuorela, M. Heinonen, E. Moilanen, Anti-inflammatory effects of flavonoids: genistein, kaempferol, quercetin, and daidzein inhibit STAT-1 and NF-κB activations, whereas flavone, isorhamnetin, naringenin, and pelargonidin inhibit only NF-κB activation along with their inhibitory effect on iNOS expression and NO production in activated macrophages, Mediators Inflamm. 2007 (2007).

[30] E.A. Middleton, X.-Y. He, F. Denorme, R.A. Campbell, D. Ng, S.P. Salvatore, M. Mostyka, A. Baxter-Stoltzfus, A.C. Borczuk, M. Loda, Neutrophil extracellular traps contribute to immunothrombosis in COVID-19 acute respiratory distress syndrome, Blood J. Am. Soc. Hematol. 136 (2020) 1169.

[31] V. Raj, J.G. Park, K.-H. Cho, P. Choi, T. Kim, J. Ham, J. Lee, Assessment of antiviral potencies of cannabinoids against SARS-CoV-2 using computational and in vitro approaches, Int. J. Biol. Macromol. 168 (2021) 474, https://doi.org/10.1016/j.ijbiomac.2020.12.020.

[32] Z. Jin, X. Du, Y. Xu, Y. Deng, M. Liu, Y. Zhao, B. Zhang, X. Li, L. Zhang, C. Peng, Y. Duan, J. Yu, L. Wang, K. Yang, F. Liu, R. Jiang, X. Yang, T. You, X. Liu, X. Yang, F. Bai, H. Liu, X. Liu, L.W. Guddat, W. Xu, G. Xiao, C. Qin, Z. Shi, H. Jiang, Z. Rao, H. Yang, Structure of M(pro) from COVID-19 virus and discovery of its inhibitors, Nature (2020), https://doi.org/10.1038/s41586-020-2223-y.

[33] L. Schrödinger, Schrödinger Suite, Schrödinger, LLC, New York, NY, 2016.

[34] R.G. Parr, W. Yang, Density functional approach to the frontier-electron theory of chemical reactivity, J. Am. Chem. Soc. 106 (1984) 4049.

[35] D. Shivakumar, J. Williams, Y. Wu, W. Damm, J. Shelley, W. Sherman, Prediction of absolute solvation free energies using molecular dynamics free energy perturbation and the OPLS force field, J. Chem. Theory Comput. 6 (2010) 1509.

[36] W. Tian, C. Chen, X. Lei, J. Zhao, J. Liang, CASTp 3.0: computed atlas of surface topography of proteins, Nucleic Acids Res. 46 (W1) (2018) W363–W367.

[37] F. Yang, X. Xiao, W. Cheng, W. Yang, P. Yu, Z. Song, Y. Yarov-Yarovoy, J. Zheng, Structural mechanism underlying capsaicin binding and activation of the TRPV1 ion channel, Nat. Chem. Biol. 11 (2015) 518.

[38] S.-Y. Huang, X. Zou, Advances and challenges in protein-ligand docking, Int. J. Mol. Sci. 11 (2010) 3016.

[39] D. Seeliger, B.L. de Groot, Ligand docking and binding site analysis with PyMOL and Autodock/Vina, J. Comput. Aided Mol. Des. 24 (2010) 417.

[40] O. Trott, A.J. Olson, AutoDock Vina: improving the speed and accuracy of docking with a new scoring function, efficient optimization, and multithreading, J. Comput. Chem. 31 (2010) 455.

[41] L. Zhang, D. Lin, X. Sun, U. Curth, C. Drosten, L. Sauerhering, S. Becker, K. Rox, R. Hilgenfeld, Crystal structure of SARS-CoV-2 main protease provides a basis for design of improved α-ketoamide inhibitors, Science 368 (2020) 409.

[42] E. Krieger, G. Vriend, New ways to boost molecular dynamics simulations, J. Comput. Chem. 36 (2015) 996.

[43] E. Krieger, R.L. Dunbrack, R.W. Hooft, B. Krieger, In Computational Drug Discovery and Design, Springer (2012) 405–421.

[44] C.J. Dickson, B.D. Madej, Å.A. Skjevik, R.M. Betz, K. Teigen, I.R. Gould, R.C. Walker, Lipid14: the amber lipid force field, J. Chem. Theory Comput. 10 (2) (2014) 865–879.

[45] S. Piotto, L. Sessa, P. Iannelli, S. Concilio, Computational study on human sphingomyelin synthase 1 (hSMS1), Biochim. Biophys. Acta Biomembr. 1859 (9) (2017) 1517–1525.

[46] M.S. Ali, J. Muthukumaran, H.A. Al-Lohedan, Molecular interactions of ceftazidime with bovine serum albumin: Spectroscopic, molecular docking, and DFT analyses, J. Mol. Liq. 313 (2020) 113490, https://doi.org/10.1016/j.molliq.2020.113490.

[47] R.G. Parr, L.v. Szentpály, S. Liu, Electrophilicity index, J. Am. Chem. Soc. 121 (9) (1999) 1922–1924.

[48] S. Jeon, M. Ko, J. Lee, I. Choi, S.Y. Byun, S. Park, D. Shum, S. Kim, Identification of antiviral drug candidates against SARS-CoV-2 from FDA-approved drugs, Antimicrob. Agents Chemother. 64 (7) (2020), https://doi.org/10.1128/AAC.00819-20.

[49] J.G. Adams, R.M. Walls, Supporting the health care workforce during the COVID-19 global epidemic, JAMA 323 (2020) 1439.

[50] J. Solnier, J.-P. Fladerer, Flavonoids: A complementary approach to conventional therapy of COVID-19?, Phytochem Rev. 20 (4) (2021) 773–795.

[51] C.-K. Tseng, H.-F. Wang, A.M. Burns, M.R. Schroeder, M. Gaspari, P.J.Cr. Baumann, Human telomerase RNA processing and quality control. Cell Rep. 13 (2015) 2232

[52] K. O'Brien, A.J. Matlin, A.M. Lowell, M.J.J.J.o.B.C. Moore, The biflavonoid isoginkgetin is a general inhibitor of Pre-mRNA splicing. J. Biol. Chem. 283 (2008) 33147

[53] A. Pawellek, U. Ryder, T. Tammsalu, L.J. King, H. Kreinin, T. Ly, R.T. Hay, R.C. Hartley, A.I.J.E. Lamond, Characterisation of the biflavonoid hinokiflavone as a pre-mRNA splicing modulator that inhibits SENP, eLife. 6 (2017), https://doi.org/10.7554/eLife.27402 e27402.

[54] S.J. Lee, K.H. Son, H.W. Chang, S.S. Kang, H.P. Kim, Inhibition of arachidonate release from rat peritoneal macrophage by biflavonoids, Arch. Pharm. Res. 20 (1997) 533.

[55] A. Pierson, R. Darrigrand, M. Rouillon, M. Boulpicante, Z.D. Renko, C. Garcia, M. Ghosh, M.-C. Laiguillon, C. Lobry, M. Alami, Splicing inhibition enhances the antitumor immune response through increased tumor antigen presentation and altered MHC-I immunopeptidome. bioRxiv (2019) 51268.1.

[56] J.M. Parks, J.C. Smith, How to discover antiviral drugs quickly, N. Engl. J. Med. 382 (2020) 2261–2264.

[57] H. Zhang, J.M. Penninger, Y. Li, N. Zhong, A.S. Slutsky, Angiotensin-converting enzyme 2 (ACE2) as a SARS-CoV-2 receptor: molecular mechanisms and potential therapeutic target, Intensive Care Med. 46 (4) (2020) 586–590.

[58] Y. Han, P. Král, Computational Design of ACE2-Based Peptide Inhibitors of SARS-CoV-2, ACS nano 14 (2020) 5143.

[59] D.R. Burton, L.M. Walker, Rational vaccine design in the time of COVID-19, Cell Host Microbe. 27 (2020) 695.

[60] Y. Jiang, W. Yin, H.E.J.B. Xu, b.r. communications, RNA-dependent RNA polymerase: Structure, mechanism, and drug discovery for COVID-19. Biochem. Biophys. Res. Commun. 538 (2021) 47

[61] M.A. Shereen, S. Khan, A. Kazmi, N. Bashir, R. Siddique, COVID-19 infection: Origin, transmission, and characteristics of human coronaviruses, J. Adv. Res. 24 (2020) 91–98.

[62] M. Romano, A. Ruggiero, F. Squeglia, G. Maga, R. Berisio, A Structural View of SARS-CoV-2 RNA Replication Machinery: RNA Synthesis, Proofreading and Final Capping. Cells 9 (2020) 1267.